Impact of modified turbulent diffusion of $PM_{2.5}$ aerosol in WRF-Chem simulations in Eastern China

Wenxing Jia[1,2], Xiaoye Zhang[2,3*]

[1]Key Laboratory for Aerosol-Cloud-Precipitation of China Meteorological Administration, Nanjing University of Information Science & Technology, Nanjing, 210044, China

[2]Key Laboratory of Atmospheric Chemistry of CMA, Chinese Academy of Meteorological Sciences, Beijing, 100081, China

[3]Center for Excellence in Regional Atmospheric Environment, IUE, Chinese Academy of Sciences, Xiamen, 361021, China

Correspondence to: X. Zhang (xiaoye@cma.gov.cn)

Abstract

Correct description of the boundary layer mixing process of particle is an important prerequisite to understanding the formation mechanism of pollutants, especially during heavy pollution episodes. Turbulent mixing process of particles is usually denoted by the turbulent diffusion of heat, which is questionable. Using mixing-length theory, a new turbulent diffusion relationship of particle is established, embedded in the model and verified on a long-term scale. The new turbulent diffusion coefficient is used to represent the turbulent mixing process of pollutants separately. Simulated results of $PM_{2.5}$ concentration were improved by 8.3% (2013), 17% (2014), 11% (2015) and 11.7% (2017) in Eastern China, respectively. Meanwhile, the new turbulent diffusion does not deteriorate the simulation results of meteorological parameters. Compared with the boundary layer height, turbulent diffusion controls the diffusion of pollutants more significantly. However, under the influence of complex topography, the turbulent

25   diffusion process is insensitive to the simulation of the pollutant concentration. For

mountainous area, the evolution of pollutants is more susceptible to advection transport.

In addition to the PM$_{2.5}$ concentration, CO as a primary pollutant, its concentration has

also been improved, which shows that the turbulent diffusion process is extremely

critical to the variation of the various aerosol pollutants.

1 Introduction

30

Along with the intensive urbanization and tremendous economic development,

numerous incidents of aerosol pollution have frequently occurred in China (An et al.,

2019; X. Zhang et al., 2019). Aerosol pollution, characterized by PM$_{2.5}$, occurs

primarily in the planetary boundary layer (PBL). The horizontal transportation and

35   vertical distribution of pollutants are obviously affected by the PBL mixing process,

associated with intricate turbulence eddies (Ren et al., 2018; Wang et al., 2018; Du et

al., 2020). Turbulent diffusion, as a vital process, controls the exchange of momentum,

heat, water vapor and pollutants through turbulence eddies within the PBL (Stull, 1988).

Moreover, the PBL height (PBLH) directly determines the effective air volume of

40   pollutant diffusion and atmospheric environmental capacity. With the continuous

development of technology, there are numerous means (e.g., radiosonde, tethered

balloon, meteorological tower, aircraft, ground-based remote sensing and space-based

remote sensing) and methods (e.g., based on surface fluxes, Richardson number and

others diagnostic methods) to determine the PBLH, of course, the results are also

45   different (Zhang et al., 2020). However, the PBLH is not necessarily negatively

correlated with pollutant concentration (Miao et al., 2021). In particular, turbulence

barrier effect can affect the vertical distribution of pollutants (Ren et al., 2021), which

make the relationship between pollutant and PBLH more uncertain. The PBLH can also

be diagnosed by the boundary layer parameterization schemes in the model, but the

50   PBLH does not directly determine the effective diffusion of pollutants (Jia and Zhang,

2020; Jia et al., 2021a). Instead, the vertical diffusion and mixing of pollutants are

2

directly determined by the turbulent diffusion coefficient (TDC), and the diagnosis of PBLH can affect the calculation of TDC. Previous studies have analyzed some pollution cases by using process analysis methods (Xing et al., 2017; Gao et al., 2018; Chen et al., 2019). The results showed that, for a pollution event, emissions and turbulent diffusion are the two processes that contribute the most to the pollutant concentration. Meanwhile, the contributions of advection transport and chemistry cannot be ignored. The evolution of pollutants is mainly controlled by turbulent diffusion, when emissions are unchanged for a short period. Therefore, more realistic turbulent diffusion characteristics are extremely important for the simulation of pollutant concentration in the model.

To date, there are still some problems need to be solved in the model, especially turbulent diffusion processes of all scalars (including active and passive scalars) are dealt with in a unified manner in the mesoscale model. Only a few studies have shown that pointed out the meteorological fields and pollutants can be changed by adjusting the minimum value of TDC (Savijarvi et al., 2002; Wang et al., 2018; Du et al., 2020; Liu et al., 2021), increasing turbulent kinetic energy (TKE) (Foreman and Emeis, 2012) and modifying experiment expressions (Sušelj and Sood, 2010; Huang and Peng, 2017). Recently, Jia et al. (2021b) obtained the TDC of particles by using high-resolution vertical flux data of particles based on the mixing length theory. Additionally, this relationship has been embedded into the WRF-Chem model to calculate the PBL mixing process of pollutants separately. This work has initially improved the overestimation of pollutant concentration at night in winter 2016 in Eastern China. However, a series of heavy pollution incidents have occurred and attracted much attention since 2013 (Miao et al., 2019). Therefore, we conducted a series of simulations for the heavy pollution periods in winter from 2013 to 2017 in this study. The difference between this study and previous work is that previous work focused on the analysis of observations, while this study mainly explores the influence of turbulent diffusion on pollutant concentration in the mesoscale model.

2 Data and methods

2.1 Data

In this study, the aerosol pollution level is denoted by the hourly surface $PM_{2.5}$ concentration that is available from the official website of the China National Environmental Monitoring Center from 1 January 2013 to 31 January 2017. $PM_{2.5}$ concentration stations increased from 35 cities in 2013(illustrated by red dots in Fig. 1b) to 78 cities in 2017(illustrated by black dots in Fig. 1b) in Eastern China. In addition to $PM_{2.5}$ observations, the hourly concentrations of CO were acquired from the National Air Quality real-time publication platform (http://106.37.208.233:20035, last access: 20 May 2021). Meanwhile, the hourly meteorological observation data, including temperature, pressure, relative humidity, wind and visibility from the national automatic weather stations (AWS) provided by the National Meteorological Information Center of China Meteorological Administration (NMICMA) (illustrated by gray crosses in Fig. 1b). The time period of the data selected is from 1 January 2013 to 31 January 2017. In addition, the turbulent diffusion of particles is calculated using high-frequency turbulence data, and observational turbulence data are obtained from the Pingyuan County Meteorological Bureau (37.15°N, 116.47°E), Shandong Province, China from 27 December 2018 to 8 January 2019 (illustrated by orange triangle in Fig. 1b). Identical eddy-covariance systems were operated, including three-dimensional sonic anemometer-thermometer (IRGASON, Campbell Scientific, USA) and CO_2/H_2O open-path gas analyzer (LI7500, LI-COR, USA). These instruments measured three components of wind speed, potential temperature, water vapor and CO_2 concentrations with a frequency of 10 Hz. The turbulence data finally was split into 30-min segments. A continuous particle measuring instrument E-sampler (Met One) and a high-frequency sampling visibility sensor CS120A (Campbell Scientific, USA) were used to obtain $PM_{2.5}$ mass concentration every minute and visibility of 1 Hz. The calculation of 30-min vertical flux of $PM_{2.5}$ is based on the nonlinear relationship between $PM_{2.5}$ concentration and visibility (Ren et al., 2020). Detailed background and calculation

4

principle of this method were presented in Ren et al. (2020), so we only describe key

steps. Firstly, we separate PM$_{2.5}$ concentration (c) and visibility datasets (V) into mean

110   and turbulent deviations (i.e., $c = \bar{c} + c'$ and $V = \bar{V} + V'$). Secondly, we get the fitted

coefficients by using exponential correlation (i.e., a and b) between the PM$_{2.5}$

concentration and visibility (i.e., $c = a \cdot V^b$). Thirdly, combining the first two steps, we

can get the turbulent fluctuations of PM$_{2.5}$ concentration (i.e., $c' = a \cdot (\bar{V} + V')^b - \bar{c}$).

Finally, we use fluctuations of vertical velocity (i.e., w') and of PM2.5 concentration

115   (i.e., c') to calculate the vertical flux of PM$_{2.5}$ (i.e., $\overline{w'c'}$).

To illustrate the influence of the PBL height (PBLH) on the PM$_{2.5}$ pollution, soundings

collected at the Fuyang site (32.54°N,115.5°E) and the Anqing site (30.37°N,116.58°E)

(illustrated by yellow pluses in Fig. 1b) for the period 2013-2017 were analyzed. These

two stations are equipped with L-band radiosonde systems (Jia et al., 2021c), which

120   proved a fine resolution (1 Hz) profiles of temperature, relative humidity and wind

speed two times (0800 and 2000 BJT) a day during winter. To eliminate the error caused

by the difference of calculation methods of PBLH, Richardson number method is used

to calculate the PBLH in both observation and simulation. The Richardson number is

defined as follows:

$$Ri(z) = \frac{g\left(\theta_{vz} - \theta_{vs}\right)\left(z - z_s\right)}{\theta_{vs}\left(u_z - u_s\right)^2 + \left(v_z - v_s\right)^2} \tag{1}$$

125   where z is the height above ground, g is the gravity, θ_v is the virtual potential

temperature, and u and v are the component of wind. The subscript "s" denotes the

surface level. The height at which the Richardson number equals 0.25 is defined as the

PBLH, which is consistent with the definition of simulation.

2.2 Numerical simulation

130 Long-term three-dimensional simulation experiments are enforced using the Weather Research and Forecasting model coupled with Chemistry (WRF-Chem version 3.9.1) (Grell et al., 2005) in this study from the winter of 2013 to 2017, when Eastern China frequently experienced severe and persistent aerosol pollution events. One month for each winter from 2013 to 2017 was selected, and a total of four months were confirmed,

135 which are January 2013, December 2014, December 2015 and January 2017, respectively. The anthropogenic emissions of BC, OC, CO, NH_3, NO_x, $PM_{2.5}$, PM_{10} and volatile organic compounds (VOCs) are set based on the latest monthly Multi-resolution Emission Inventory for China (MEIC) from 2013 to 2017 are provided by Tsinghua University, with a resolution of $0.25°×0.25°$ (http://meicmodel.org/, last

140 access: 20 May 2021). The model domain was centered over Eastern China with a horizontal resolution of 33 and 6.6 km (Fig. 1a). The model top was set to the 50 hPa level, and 48 vertical layers were configured below the top. To resolve the PBL structure, 21 vertical layers were set below 2 km (Above Ground Level, AGL). The physics parameterization schemes selected for this study included the Morrison double-

145 moment microphysics scheme (Morrison et al., 2009), RRTMG longwave/shortwave radiation schemes (Iacono et al., 2008), MM5 similarity surface layer scheme (Jiménez et al., 2012), Noah land surface scheme (Chen and Dudhia, 2001), Singer-layer UCM scheme (Kusaka et al., 2001), CLM4.5 lake physics scheme (Subin et al., 2012; Gu et al., 2015), ACM2 planetary boundary layer scheme (Pleim, 2007), Grell-3D cumulus

150 scheme (Grell and Devenyi, 2002). And the chemical mechanism is the RADM2-MADE/SORGM scheme (Ackermann et al., 1998; Schell et al., 2001). The initial and boundary conditions of meteorological fields were set up using the National Centers for Environmental Prediction (NCEP) global final (FNL) reanalysis data, with a resolution of $1°×1°$ (https://rda.ucar.edu/datasets/ds083.2/, last access: 20 May 2021). And the

155 initial and boundary conditions of chemical fields were configured using the global

model output of Model for Ozone and Related Chemical Tracers (MOZART) (http://www/acom.ucar.edu/wrf-chem/mozart.shtml, last access: 20 May 2021).

Simulation using abovementioned configurations is referred to as the original runs. In the original PBL parameterization scheme, TDCs of heat and momentum are different (i.e., $K_h \neq K_m$). The turbulent mixing process of pollutants is considered to be similar to that of heat, which supposes the turbulent diffusions of particles and heat are identical (i.e., $K_h=K_c$). While in the improved scheme, the turbulent mixing process of pollutants is calculated by the TDC of particles (i.e., K_c), which is different from TDC of heat (i.e., $K_h \neq K_c$). These improved experiments are regarded as the new runs hereafter. All simulation included a total of eight months. The 91-h simulation is conducted beginning from 0000UTC of three days ago for each day (i.e., 248 simulation experiments), and first 64-h of each simulation is considered as the spin-up period.

2.3 Calculation principle of turbulent diffusion of particles

Considering that the pollution is usually accompanied by the stable boundary layer (SBL), and the simulation results of pollutant concentration are poor in the SBL at night. Thus, we mainly modify the program of the stable boundary layer, while for the unstable boundary layer, we still use the default program of the original scheme.

The TDC is parameterized by the mixing length (l) and the function of Richardson number ($f(Ri)$) based on Mixing length theory, that is

$$K = 0.01 + \sqrt{ss} \cdot l^2 \cdot f(Ri) \tag{2}$$

where ss is the wind shear (i.e., $ss = (\partial u/\partial z)^2 + (\partial v/\partial z)^2$), 0.01 refers to the minimum value of TDC in the model. The mixing length formula (i.e., $l = \kappa z/(1+\kappa z/\lambda)$, $\lambda=80$) proposed by Blackadar (1962), and it is widely used in the model (Louis, 1979; Lin et al., 2008; Pleim, 2016). Many previous studies have showed various functions of Richardson number, which represent the different situations of turbulence. Here, we

180　　mainly compare the similarities and differences between the turbulent diffusion of momentum, heat and particles in the model.

(i) For the stable conditions (i.e., $Ri \geq 0$), Esau and Byrkjedal (2007) suggested:

$$f_h = (1 + 10Ri + 50Ri^2 + 5000Ri^4)^{-1} + 0.0012 \qquad (3)$$

$$f_m = 0.8f_h + 0.00104 \qquad (4)$$

where f_h and f_m denote the functions of heat and momentum, respectively, and these functions have been implemented in the original model. We added an additional

185　　function of particles into the model, that is

$$f_c = (1 + 66.6Ri)^{-1} \qquad (5)$$

which is used to denote the turbulent mixing process of particles within the PBL. When Ri is greater than ~0.2, the TDC of particles is greater than that of heat, which may reduce pollutant concentration. With the increase of instability, the TDC of particles is gradually smaller than that of heat, which theoretically leads to the increase of pollutant

190　　concentration. For detailed analysis and comparison of functions, please refer to Jia et al. (2021b).

(ii) For the unstable conditions ($Ri < 0$):

$$f_h = f_c = (1 - 25Ri)^{1/2} \qquad (6)$$

$$f_m = \mathrm{Pr} \cdot f_h \qquad (7)$$

where the TDC of particles is still equal to that of heat, while the TDC of momentum is calculated by turbulent Prandtl number (i.e., Pr, Pr=0.8).

195　　There are several important information about the TDC of particles that need to be illustrated. (1) Turbulent diffusion of particles calculated by the explicit local gradient to represent the PBL mixing process of particles, which are more suitable in the stable boundary layer (SBL) (Mahrt and Vickers, 2003). (2) The new scheme avoids the inapplicability of the Monin-Obukhov similarity theory (MOST), the deviation of the

200　　PBLH in the SBL, and higher computational efficiency (Li et al., 2010), and it is easier

to applied to the forecasting models in the future. (3) Turbulent diffusion of particles is used to evaluate the PBL mixing process of pollutants separately, which can affect the simulation results of pollutants and not influence the simulation results of meteorological parameters.

3 Evaluation of PM$_{2.5}$ concentration simulation

Based on the TDC relationship of particles in the previous study (Jia et al., 2021b), this study applies this relationship to a long-term scale simulation for verification. Figure 2 shows the average value of simulated and observed PM$_{2.5}$ concentration at night from 2013 to 2017, and the simulation results can better reproduce the distribution of pollutant concentration (i.e., represented by the red dashed circle). However, the PM$_{2.5}$ concentration was overestimated in varying degrees in Eastern China (i.e., indicated by the green dashed circle), and the mean relative bias (RB) of the region is as high as 11.8% (2013), 48% (2014), 23.8% (2015) and 20.9% (2017), respectively (Fig. 2i-l). In addition, we also found that the pollutant concentrations are underestimated in Beijing (BJ) and along the Taihang Mountains (Mt. Taihang) (i.e., indicated by the purple irregular circle), but overestimated in Tianjin (TJ) (Fig. 2i-l). What are the reasons for the pollutant concentration simulated by the same model are different in various regions? What are the different effects of turbulent diffusion in various regions? These issues will be further explained later, and this section mainly evaluates the simulation results of the pollutant concentration. Compared to the original scheme, the new scheme improves the situation where the pollutant concentration is overestimated at night in Eastern China (Fig. 3a-d). The degree of overestimation of the pollutant concentration is reduced, and the mean relative bias of the new scheme is 3.5% (2013), 31% (2014), 12.8% (2015) and 9.2% (2017), respectively (Fig. 3e-h). Moreover, the mean absolute bias is reduced by 8.3% (2013), 17% (2014), 11% (2015) and 11.7% (2017), respectively (Fig. 3i-l). In summary, compared with the original scheme, the new scheme can generally improve the overestimation of pollutant concentration in Eastern China, which is due to the improvement of turbulent diffusion. For the previously

mentioned stations where underestimated the pollutant concentration in the original scheme, the pollutant concentration will be further underestimated with the increase of turbulent diffusion. However, this underestimation cannot be avoided because there is an opposite phenomenon in the pollutant concentration of the two regions. We can only look at the differences in the two regions from other perspectives (see section 4 for details), due to there are many uncertainties in the model.

To better evaluate the model performance, Figure 4 shows the Taylor diagram of hourly $PM_{2.5}$ concentration, and the black (red) dots indicate original (new) simulation results at all stations from 2013 to 2017. The statistical results present a consistent feature, that is, the worse the simulation results of the original scheme are, the more obvious improvement of the new scheme becomes (arrows indicate improved stations in the Fig. 4). The results indicate that the pollutant concentrations at all stations are not improved to the same extent. When the simulation of pollutant concentration is overestimated by the original scheme, the new scheme will significantly reduce the degree of overestimation. While the simulation of pollutant concentration is underestimated by the original scheme, the new scheme will not further underestimate with the previous changing and the degree of re-underestimate is not obvious (Fig. 4). And the standard deviation (normalized) of the mean value is decreased by 0.2 (2013), 0.28 (2014), 0.14 (2015) and 0.16 (2017) (Fig. 4). As a whole, the new scheme can significantly improve the common phenomenon of overestimated pollutant concentration in the SBL in Eastern China (Fig. 4).

With the increase of turbulent diffusion, the pollutant concentration decreases gradually. Where do the reduced pollutants go? Did it spread to the surrounding area in the horizontal direction or to the upper level in the vertical direction? This question deserves further discussion. It can be seen from Figure 3 that the reduction of pollutant concentration is a regional synchronous change, and there is no regular concentration gradient in the horizontal direction. Therefore, we should also pay more attention to the changes in the vertical direction. Theoretically, increasing turbulent diffusion will

reduce the pollutant concentrations near the surface-layer, and the pollutants will be more fully mixing in the vertical direction, which results in lower concentrations of pollutants in the near surface-layer and higher concentrations of pollutants in the upper layer. As we expected, the pollutant concentration is reduced in the surface-layer and it is increased in the upper layer at night (Fig. 5), which is consistent with the theory.

4 Uncertainty analysis

4.1 Meteorological parameters

Depending on high-frequency particle flux, the TDC of particles has been added in the model to calculate the turbulent mixing process of particles separately. Compared with previous studies on the improvement of parameterization scheme, the greatest strengths of the new scheme are that not only improves the simulation results of pollutant concentration, but also does not deteriorate the simulation results of other parameters. To verify the new scheme does not affect the simulation results of the meteorological parameters, the simulation results of the near-surface meteorological elements (i.e., 2-m temperature, 2-m relative humidity and 10-m wind speed) between original and new schemes have been compared and analyzed. It can be seen from Figure S1-S3 that the correlation coefficients of meteorological parameters by two schemes are greater than 0.99, noting that the new scheme does not alter the performance of meteorological fields, which is an advantage of the new scheme. As mentioned earlier, modifying the turbulent diffusion coefficient of heat not only affects the simulation of temperature (Savijarvi and Kauhanen, 2002), but also influences the results of pollutants (Liu et al., 2021). Improving the parameterization scheme is a long and tough process, making it difficult to improve the simulation results of all parameters at once. When the simulation results of one parameter are improved, we should first seek to ensure that the simulation results of other parameters are not deteriorated. Then, we are going to look at improving other parameters. Although the aerosol-radiation two-way feedback process has been considered in the WRF-Chem model, the change of $PM_{2.5}$ concentration caused by

radiation feedback is only a few percentage (Li et al., 2017; Wu et al., 2019; Gao et al.,

285   2020). We should focus more on the feedback process between turbulence and aerosol,

and hopefully develop a turbulence-aerosol two-way feedback module. Some turbulent

characteristics (e.g., turbulence barrier effect) can be taken into consideration during

HPEs, reflecting a more realistic evolution process of pollutant concentration. We will

further clarify the relationship between particles, momentum and heat transport through

290   observational data, so as to lay the foundation for the improvement of the model.

4.2 PBL height

Although PBL height (PBLH) is widely used to determine the effective air volume and

atmospheric environmental capacity for pollutant diffusion, various methods diagnose

different PBLH, which reinforces uncertainty about the PBLH as a criterion. When

295   there is a transport stage with a high wind speed during HPEs, the mechanical

turbulence is strong, and the PBLH and pollutant concentration increase simultaneously

(Jia et al., 2021c; Miao et al. 2021). Therefore, the relationship between PBLH and

$PM_{2.5}$ pollution is intricate. The impact of PBLH is ultimately represented through the

TDC in the model, because the PBLH is used to calculate TDC (Jia et al., 2021b), and

300   artificial changing PBLH can also affect the simulation of pollutant concentration. If

the simulation error of pollutant concentration is caused by the PBLH, that is the

pollutant concentration is overestimated and the PBLH should be underestimated.

However, the PBLH is reproduced well by the model, and the model does not

underestimate the PBLH (Fig. 6). Anqing is located in the mountain corridor, the

305   simulation results of PBLH (Index of agreement, IOA=0.49~0.81) is slightly worse

than that in Fuyang (IOA=0.63~0.85). Therefore, various factors will influence the

calculation of PBLH. A more accurate PBLH can indeed reduce some uncertainty of

the model, but how to apply the accurate PBLH through observation to the model is a

thorny problem. For example, the turbulence barrier effect changes the mixing height

310   of pollutants (Ren et al., 2021), which cannot be reflected in the model and can lead to

deviation in the simulation of pollutant concentration. The new scheme does not disturb

the simulation results of meteorological fields, thus, does not affect the simulation results of PBLH (Fig. S4). The simulation results of pollutant concentrations are improved under the similar PBLH, which further demonstrates that the simulation of

315   pollutant concentration is not only controlled by the PBLH, but also influenced by turbulent diffusion. In the final analysis, turbulent diffusion controls the diffusion of pollutant concentration and the evolution of meteorological parameters.

4.3 Influence of other processes

Overestimating of pollutant concentrations has been improved in Eastern China, but

320   there are also some sites in northern China where pollutant concentrations are underestimated (Fig. 2i-l). These sites (i.e., Hebei and Beijing) are mostly located in the east of the Taihang Mountains and the south of the Yan Mountains (Fig. 7). For example, in December 2016, the pollutant concentrations of all sites in Beijing were not underestimated. Jia et al. (2021b) have found that the pollutant concentrations of

325   two sites located in the south of Beijing (i.e., blue dots in Fig. S2 in Jia et al., 2021b) are well reproduced by the model. This phenomenon also occurred in 2013-2017 (Fig. 7), and the pollutant concentrations were significantly underestimated at some sites, which are close to the mountainous area. The boundaries of overestimated and underestimated sites are pronounced in Beijing-Tianjin-Hebei region (white dashed in

330   Fig. 7), and the pollutant concentration is overestimated at some sites, which are away from the mountainous area (i.e., Tianjin and southeast of Hebei). Meanwhile, the TDC of the new scheme is greater than that of the original scheme in Eastern China (i.e., red dashed circle in Fig. 8i-l), that is, the increased turbulent diffusion reduces the overestimation of pollutant concentration in this area. Furthermore, we found that the

335   TDC of the new scheme is significantly smaller than that of the original scheme in the mountainous area (i.e., green irregular circle in Fig. 8). Theoretically, the reduced TDC should increase the pollutant concentration, and improve the underestimation of pollutant concentration in the original scheme. Disappointingly, the change of TDC does not improve the underestimation of pollutant concentration in the mountainous

340   area (Fig. 7, 8i-l), which indicates that the change of turbulent diffusion is not sensitive

to the pollutant concentration in the mountainous area.

In addition to the two main influencing factors of emission and turbulent diffusion, advection transport and chemistry processes can also affect the simulation of pollutant concentration. Since we use the latest emissions source inventory, there is no way to

345   use other more elaborate inventories to quantify the uncertainty caused by emissions. Advection process, is highly related to wind and $PM_{2.5}$ concentration gradients from upwind areas to downwind areas (Gao et al., 2018). Figure 9 shows that the simulation results of wind speed, and we found that the wind speed is overestimated in the whole simulation area, which is also the systematic deviation of the model (Jia and Zhang,

350   2020). However, there are regional differences in the overestimation of wind speed, which is more obvious in areas with complex terrain (framed by purple lines in Fig. 9). Jimenez and Dudhia (2012) indicated that the overestimation of wind speed may be caused by the incorrect describe sub-grid surface roughness. For the purple rectangle region, although the wind speed is overestimated, there is no obvious wind speed

355   gradient and pollutant concentration gradient (Fig. 2a-d, 9a-d). Thus, the effect of advection is not significant. While for the irregular purple region, we can see that the obvious wind speed gradient and pollutant concentration gradient (Fig. 2a-d, 9a-d). In the northwest of the irregular purple area, clean air will pass through this area under the control of stronger northwesterly wind. Therefore, this area is extremely likely to be

360   affected by advection transport, so that the pollutant concentration has been underestimated in this area. We should pay more attention to the improvement of wind field simulation on complex terrain and we expect that the simulation of wind field will be improved and the pollutant concentration in this area will also be improved.

Chemistry process, i.e., the $PM_{2.5}$ concentration contribution caused by secondary

365   transformation, was negligible in this study, and is not mentioned further in this paper. Whether the simulation of chemical components has been improved, it cannot be well verified due to lack of observational data. Although the simulation results of $PM_{2.5}$

14

components are not capable of being evaluated, CO, as a representative of primary pollutants, can be compared to the observations. Results from new scheme with TDC of particles are more consistent with the observations than the original scheme (Fig. S5), which supports the improvement of $PM_{2.5}$ concentration (Fig. 4 and S5). In addition, the dry deposition process of particles is also extremely important (Zhang et al., 2001; Farmer et al., 2021). The turbulent mixing and dry deposition processes belong to the same main program in the mesoscale model. However, with increasing particle size, particle inertia and gravity cannot be neglected, but these inertia and gravity effects are neglected for particles smaller than 10 µm in diameter (Fratini et al., 2007). Therefore, we did not involve the influence of gravity on pollutant concentration in this study. In the future, we should use long-term simulation results to verify the difference of aerosol process decomposition in detail.

5 Conclusions and prospects

At present, mesoscale model is facing numerous challenges, especially during heavy pollution episodes. One of these challenges is the correct describe the turbulent mixing process of pollutants. Although the model can reproduce the evolution of pollutants, the simulation of diurnal variation of pollutants is fundamentally flawed, especially at night. Errors in estimation of pollutant concentration are primarily caused by defects in the turbulent mixing of pollutants in the model. Actually, there is a difference between the turbulent transport of heat and particles. This result inspires us to deal with the turbulent diffusion of heat and particles separately. Therefore, based on the turbulent diffusion expression of particles proposed by Jia et al., 2021b, we again demonstrated the improvement of pollutant concentration in winter from 2013 to 2017, and the uncertainty factors are also analyzed in the model.

The original scheme overestimates the surface $PM_{2.5}$ concentration by 11.8% (2013), 48% (2014), 23.8% (2015) and 20.9% (2017) at night, respectively. The new scheme has improved the overestimation of the surface $PM_{2.5}$ concentration in eastern China at

night, and the mean absolute bias of the region can be reduced by 8.3% (2013), 17% (2014), 11% (2015) and 11.7% (2017), respectively. In the horizontal direction, the pollutant concentration showed regional synchronous changes. Therefore, the pollutant concentration is reduced near the surface and better mixed in the whole layer, increasing the pollutant concentration in the upper level. Moreover, the new scheme not only improves the simulation of pollutant concentration, but also does not deteriorate the simulation of other meteorological parameters. Although the PBLH affects the diffusion of pollutants, the simulation of pollutant concentration is not specifically controlled by the PBLH, but effected by TDC. It is worth noting that TDC has a negligible impact on the simulation of pollutant concentration at some sites with complex topography. Meanwhile, advection transport may dominate the evolution of pollutant concentration in mountainous area. The simulation results of $PM_{2.5}$ components cannot be evaluated, due to lack of observational data. CO, however, as a representative of primary pollutants, can be compared to observations. Results from new scheme are more consistent with the observations than the original scheme, which supports the improvement of $PM_{2.5}$ concentration.

The new scheme could provide promising guidance during heavy pollution episodes. The turbulent transport mechanism and turbulent parameterization is a complex topic (Lemon et al., 2019; Couvreux et al., 2020; Edwards et al., 2020), and beyond that, other processes (or other parameters) also need in-depth understanding and exploration (Zhang et al., 2001; Seinfeld et al., 2016; Shao et al., 2019; Emerson et al., 2020). Therefore, more research during the heavy pollution episodes, especially on the experimental side (e.g., carry out extensive measurement campaigns), might shed more light on the turbulent mixing process and transport mechanisms of pollutants.

Data availability

The surface $PM_{2.5}$ concentration, meteorological data, turbulent datasets and turbulent flux data of $PM_{2.5}$ are available by request (xiaoye@cma.gov.cn).

Author contributions

Development of the ideas and concepts behind this work was performed by all the authors. Model execution, data analysis and paper preparation were performed by WJ and XZ with feedback and advice.

Competing interests

The authors declare that they have no conflict of interest.

References

Ackermann, I. J., Hass, H., Memmesheimer, M., Ebel, A., Binkowski, F. S., and Shankar, U.: Modal aerosol dynamics model for Europe, Atmos. Environ., 32, 2981–2999, https://doi.org/10.1016/S1352-2310(98)00006-5, 1998.

An, Z., Huang, R., Zhang, R., Tie, X., Li, G., Cao, J., Zhou, W., Shi, Z., Han, Y., Gu, Z., and Ji, Y.: Severe haze in northern China: A synergy of anthropogenic emissions and atmospheric processes, P. Natl. Acad. Sci. USA, 116, 8657–8666, https://doi.org/10.1073/pnas.1900125116, 2019.

Blackadar, A. K.: The vertical distribution of wind and turbulent exchange in a neutral atmosphere, J. Geophys. Res., 67, 3095–3102, https://doi.org/10.1029/JZ067i008p03095, 1962.

Chen, F., and Dudhia, J.: Coupling an advanced land surface – hydrology model with the Penn State – NCAR MM5 modeling system. Part I: model implementation and sensitivity, Mon. Wea. Rev., 129, 569–585, https://doi.org/10.1175/1520-0493(2001)129 < 0587:CAALSH > 2.0.CO, 2, 2001.

Chen, L., Zhu, J., Liao, H., Gao, Y., Qiu, Y., Zhang, M., Liu, Z., Li, N., and Wang, Y.: Assessing the formation and evolution mechanisms of severe haze pollution in the Beijing–Tianjin–Hebei region using process analysis, Atmos. Chem. Phys., 19, 10845-10864, https://doi.org/10.5194/acp-19-10845-2019, 2019.

450 Couvreux, F., Bazile, E., Rodier, Q., Maronga, B., Matheou, G., and Chinita, M. J., Edwards, J., Stratum, B. J. H., van Heerwaarden, C. C., Huang, J., Moene, A. F., Cheng, A., Fuka, V., Basu, S., Bou-Zeid, E., Canut, G., and Vignon, E.: Intercomparison of large-eddy simulations of the Antarctic boundary layer for very stable stratification, Bound.-Lay. Meteorol., 176, 369–400, https://doi.org/10.1007/s10546-020-00539-4, 2020.

455 Du, Q., Zhao, C., Zhang, M., Dong, X., Cheng, Y., Liu, Z., Hu, Z., Zhang, Q., Li, Y., Yuan, R., and Miao, S.: Modeling diurnal variation of surface $PM_{2.5}$ concentrations over East China with WRF-Chem: impacts from boundary-layer mixing and anthropogenic emission, Atmos. Chem. Phys., 20, 2839–2863, https://doi.org/10.5194/acp-20-2839-2020, 2020.

Edwards, J. M., Beijaars, A. C., Holtslag, A. A., and Lock, A. P.: Representation of boundary-layer
460 processes in numerical weather prediction and climate models, Bound.-Lay. Meteorol., 177, 511–539, https://doi.org/10.1007/s10546-020-00530-z, 2020.

Emerson, E. W., Hodshire, A. L., Debolt, H. M., Bilsback, K. R., Pierce, J. R., McMeeking, G. R., and Farmer, D. K.: Revisiting particle dry deposition and its role in radiative effect estimates, P. Natl. Acad. Sci. USA, 117, 26076–26082, https://doi.org/10.1073/pnas.2014761117, 2020.

465 Esau, I. N., and Byrkjedal, Ø.: Application of large eddy simulation database to optimization of first order closure for neutral and stably stratified boundary layers, Bound.-Lay. Meteorol., 125, 207–225, https://doi.org/10.1007/s10546-007-9213-6, 2007.

Farmer, D.K., Boedicker, E.K. and DeBolt, H.M.: Dry Deposition of Atmospheric Aerosols: Approaches, Observations, and Mechanisms, Annu. Rev. Phys. Chem. 72, 16.1–16.23,
470 https://doi.org/10.1146/annurev-physchem-090519-034936, 2021.

Foreman, R. J., and Emeis, S.: A Method for Increasing the Turbulent Kinetic Energy in the Mellor–Yamada–Janjić Boundary-Layer Parametrization, Bound.-Lay. Meteorol., 145, 329–349, https://doi.org/10.1007/s10546-012-9727-4, 2012.

Fratini, G., Ciccioli, P., Febo, A., Forgione, A., and Valentini, R.: Size-segregated fluxes of mineral dust
475 from a desert area of northern China by eddy covariance. Atmos. Chem. Phys., 7, 2839–2854, https://doi.org/10.5194/acp-7-2839-2007, 2007.

Gao, J., Zhu, B., Xiao, H., Kang, H., Pan, C., and Wang, D., and Wang, H.: Effects of black carbon and boundary layer interaction on surface ozone in Nanjing, China, Atmos. Chem. Phys., 18, 7081–7094, https://doi.org/10.5194/acp-18-7081-2018, 2018.

480   Gao, M., Han, Z., Tao, Z., Li, J., Kang, J.-E., Huang, K., Dong, X., Zhuang, B., Li, S., Ge, B., Wu, Q., Lee, H.-J., Kim, C.-H., Fu, J. S., Wang, T., Chin, M., Li, M., Woo, J.-H., Zhang, Q., Cheng, Y., Wang, Z., and Carmichael, G. R.: Air quality and climate change, Topic 3 of the Model Inter-Comparison Study for Asia Phase III (MICS-Asia III) – Part 2: aerosol radiative effects and aerosol feedbacks, Atmos. Chem. Phys., 20, 1147–1161, https://doi.org/10.5194/acp-20-1147-2020, 2020.

485   Grell, G. A., and Devenyi, D.: A generalized approach to parameterizing convection combining ensemble and data assimilation techniques, Geophys. Res. Lett., 29, 1693, https://doi.org/10.1029/2002GL015311, 2002.

Grell, G.A., Peckham, S.E., Schmitz, R., McKeen, S.A., Frost, G., Skamarock, W.C., and Eder, B.: Fully coupled "online" chemistry within the WRF model. Atmos. Environ., 39, 6957–6975.
490   https://doi.org/10.1016/j.atmosenv.2005.04.027, 2005.

Gu, H., Jin, J., Wu, Y., Ek, M. B., and Subin, Z. M.: Calibration and validation of lake surface temperature simulations with the coupled WRF-lake model, Clim. Change., 129, 471–483, https://doi.org/10.1007/s10584-013-0978-y, 2015.

Huang, Y., and Peng, X.: Improvement of the Mellor–Yamada–Nakanishi–Niino Planetary Boundary-
495   Layer Scheme Based on Observational Data in China, Bound.-Lay. Meteorol., 162, 171–188, https://doi.org/10.1007/s10546-016-0187-0, 2017.

Iacono, M. J., Delamere, J. S., Mlawer, E. J., Shephard, M. W., Clough, S. A., and Collins, W. D.: Radiative forcing by long-lived greenhouse gases: calculations with the AER radiative transfer models, J. Geophys. Res.: Atmos., 113, D13103. https://doi.org/10.1029/2008JD009944, 2008.

500   Jia, W., and Zhang, X.: The role of the planetary boundary layer parameterization schemes on the meteorological and aerosol pollution simulations: A review, Atmos. Res., 239, 104890, https://doi.org/10.1016/j.atmosres.2020.104890, 2020.

Jia, W., Zhang, X., and Wang, Q.: Assessing the pollutant evolution mechanisms of heavy pollution episodes in the Yangtze-Huaihe valley: A multiscale perspective, Atmos. Environ., 244, 117986,
505   https://doi.org/10.1016/j.atmosenv.2020.117986, 2021a.

Jia, W., Zhang, X., Zhang, H., and Ren, Y.: Application of turbulent diffusion term of aerosols in mesoscale model, Geophys. Res. Lett., 48, e2021GL093199, https://doi.org/10.1029/2021GL093199, 2021b.

Jia, W., Zhang, X., Wang, J., Yang, Y., and Zhong, J.: The influence of stagnant and transport types
510   weather on heavy pollution in the Yangtze-Huaihe valley, China, Sci. Total Environ., 792, 148393, https://doi.org/10.1016/j.scitotenv.2021.148393, 2021c.

Jiménez, P.A., Dudhia, J.: Improving the representation of resolved and unresolved topographic effects on surface wind in the WRF model, J. Appl. Meteorol. Climatol., 51, 300–316, https://doi.org/10.1175/JAMC-D-11-084.1, 2012.

515 Jiménez, P. A., Dudhia, J., González–Rouco, J. F., Navarro, J., Montávez, J. P., and García–Bustamante E.: A revised scheme for the WRF surface layer formulation, Mon. Wea. Rev., 140, 898–918, https://doi.org/10.1175/MWR-D-11-00056.1, 2012.

Kusaka, H., Kondo, H., Kikegawa, Y., and Kimura, F.: A simple single-layer urban canopy model for atmospheric models: comparison with multi-layer and slab models. Bound.-Lay. Meteorol., 101,
520   329–358, https://doi.org/10.1023/a:1019207923078, 2001.

LeMone, M. A., Angevine, W. M., Bretherton, C. S., Chen, F., Dudhia, J., Fedorovich, E., Katsaros, K. B., Lenschow, D. H., Mahrt, L., Patton, E. G, Sun, J. L., Tjernström, M., and Weil, J.: 100 Years of progress in boundary layer meteorology, Meteorol. Mono., 59, 9.1–9.85, https://academic.microsoft.com/paper/2935666247, 2019.

525 Li, M., Wang, T., Xie, M., Zhuang, B., Li, S., Han, Y., and Chen, P.: Impacts of aerosol-radiation feedback on local air quality during a severe haze episode in Nanjing megacity, eastern China, Tellus B: Chem. Phys. Meteorol., 69, 1339548, https://doi.org/10.1080/16000889.2017.1339548, 2017.

Li, Y., Gao, Z., Lenschow, D. H., and Chen, F.: An improved approach for parameterizing surface-layer turbulent transfer coefficients in numerical models, Bound.-Lay. Meteorol., 137, 153–165,
530   https://doi.org/10.1007/s10546-010-9523-y, 2010.

Lin, J., Youn, D., Liang, X., and Wuebbles, D. J.: Global model simulation of summertime U.S. ozone diurnal cycle and its sensitivity to PBL mixing, spatial resolution, and emissions, Atmos. Environ., 42, 8470–8483, https://doi.org/10.1016/j.atmosenv.2008.08.012, 2008.

Liu, C., Huang, J. Hu, X.-M., Hu, C., Wang, Y., Fang, X., Luo, L., Xiao, H., and Xiao, H.: Evaluation of
535   WRF-Chem simulations on vertical profiles of $PM_{2.5}$ with UAV observations during a haze pollution event, Atmos. Environ., 252, 118332, https://doi.org/10.1016/j.atmosenv.2021.118332, 2021.

Louis, J.: A parametric model of vertical eddy fluxes in the atmosphere, Bound.-Lay. Meteorol., 17, 187–202, https://doi.org/10.1007/BF00117978, 1979.

Mahrt, L., and Vickers, D.: Formulation of turbulent fluxes in the stable boundary layer, J. Atmos. Sci.,

540   60, 2538–2548, https://doi.org/10.1175/1520-0469(2003)060<2538:FOTFIT>2.0.CO;2, 2003.

Miao, Y., Che, H., Zhang, X., and Liu, S.: Relationship between summertime concurring $PM_{2.5}$ and O_3

pollution and boundary layer height differs between Beijing and Shanghai, China, Environ. Pollut.,

268, 115775, https://doi.org/10.1016/j.envpol.2020.115775, 2021.

Miao, Y., Li, J., Miao, S., Che, H., Wang, Y., Zhang, X., Zhu, R., and Liu, S.: Interaction between

545   planetary boundary layer and PM2.5 pollution in megacities in China: a review, Curr. Pollut. Rep.,

5, 261–271, https://doi.org/10.1007/s40726-019-00124-5, 2019.

Morrison, H., Thompson, G., and Tatarskii, V.: Impact of Cloud Microphysics on the Development of

Trailing Stratiform Precipitation in a Simulated Squall Line: Comparison of One– and Two–

Moment Schemes, Mon. Wea. Rev., 137, 991–1007, https://doi.org/10.1175/2008MWR2556.1,

550   2009.

Pleim, J. E.: A combined local and nonlocal closure model for the atmospheric boundary layer. Part I:

model   description   and   testing,   J.   Appl.   Meteorol.   Climatol.,   46,   1383–1395,

https://doi.org/10.1175/JAM2539.1, 2017.

Pleim, J. E., Gilliam, R., Appel, W., and Ran, L.: Recent advances in modeling of the atmospheric

555   boundary layer and land surface in the coupled WRF-CMAQ model, Air Pollution Modeling and its

Application XXIV, 391–396, https://doi.org/10.1007/978-3-319-24478-5_64, 2016.

Ren, Y., Zhang, H., Wei, W., Cai, X., and Song, Y.: Determining the fluctuation of $PM_{2.5}$ mass

concentration and its applicability to Monin–Obukhov similarity, Sci. Total Environ., 710, 136398,

https://doi.org/10.1016/j.scitotenv.2019.136398, 2020.

560 Ren, Y., Zhang, H., Zhang, X., Wei, W., Li, Q., Wu, B., Cai, X., Song, Y., Kang, L., and Zhu, T.:

Turbulence barrier effect during heavy haze pollution events, Sci. Total Environ., 753, 142286,

https://doi.org/10.1016/j.scitotenv.2020.142286, 2021.

Ren, Y., Zheng, S., Wei, W., Wu, B., Zhang, H., Cai, X., and Song, Y.: Characteristics of the turbulent

transfer during the heavy haze in winter 2016/17 in Beijing, J. Meteor. Res., 32, 69–80,

565   https://doi.org/10.1007/s13351-018-7072-3, 2018.

Savijärvi, H., and Kauhanen, J.: High resolution numerical simulations of temporal and vertical

variability in the stable wintertime boreal boundary layer: a case study, Theor. Appl. Climaol., 70,

97–103, https://doi.org/10.1007/s007040170008, 2002.

Schell, B., Ackermann, I. J., and Hass, H.: Modeling the formation of secondary organic aerosol within a comprehensive air quality model system, J. Geophys. Res., 106, 28275–28293, https://doi.org/10.1029/2001JD000384, 2001.

Seinfeld, J. H., Bretherton, C., Carslaw, K. S., Coe, H., DeMott, P. J., Dunlea, E. J., Feingold, G., Ghan, S., Guenther, A. B., Kahn, R., Kraucunas, I., Kreidenweis, S. M., Molina, M. J., Nenes, A., Penner, J. E., Prather, K. A., Ramanathan, V., Ramaswamy, V., Rasch, P. J., Ravishankara, A. R., Rosenfeld, D., Stephens, G., and Wood, R.: Improving our fundamental understanding of the role of aerosol-cloud interactions in the climate system, P. Natl. Acad. Sci. USA, 113, 5781–5790. https://doi.org/10.1073/pnas.1514043113, 2016.

Shao, J., Chen, Q, Wang, Y., Lu, X., He, P., Sun, Y., Shah, V., Martin, R. V., Philip, S., Song, S., Zhao, Y., Xie, Z., Zhang, L., and Alexander, B.: Heterogeneous sulfate aerosol formation mechanisms during wintertime Chinese haze events: air quality model assessment using observations of sulfate oxygen isotopes in Beijing, Atmos. Chem. Phys., 19, 6107–6123. https://doi.org/10.5194/acp-19-6107-2019, 2019.

Smedman, A.-S., Högström, U., Hunt, J. C. R., and Sahlée, E.: Heat/mass transfer in the slightly unstable atmospheric surface layer, Q. J. R. Meteorol. Soc. 133, 37–51. https://doi.org/10.1002/qj.7, 2007.

Stull, R. B.: An introduction to boundary layer meteorology, Atmospheric Sciences Library, 6, 206–210, 1988.

Subin, Z. M., Riley, W. J., and Mironov, D.: An improved lake model for climate simulations: Model structure, evaluation, and sensitivity analyses in CESM1, J. Adv. Model. Earth Syst., 4, M02001, https://doi.org/10.1029/2011MS000072, 2012.

Sušelj, K., and Sood, A.: Improving the Mellor–Yamada–Janjić Parameterization for wind conditions in the marine planetary boundary layer, Bound.-Lay. Meteorol., 136, 301–324. https://doi.org/10.1007/s10546-010-9502-3, 2010.

Wang, H., Peng, Y., Zhang, X., Liu, H., Zhang, M., Che, H., Cheng, Y., and Zheng, Y.: Contributions to the explosive growth of $PM_{2.5}$ mass due to aerosol-radiation feedback and decrease in turbulent diffusion during a red alert heavy haze in Beijing-Tianjin-Hebei, China, Atmos. Chem. Phys. 18, 17717–17733. https://doi.org/10.5194/acp-18-17717-2018, 2018.

Wu, J., Bei, N., Hu, B., Liu, S., Zhou, M., Wang, Q., Li, X., Liu, L., Feng, T., Liu, Z., Wang, Y., Cao, J., Tie, X., Wang J., Molina, L. T., and Li, G.: Aerosol–radiation feedback deteriorates the wintertime

haze in the North China Plain, Atmos. Chem. Phys., 19, 8703–8719, https://doi.org/10.5194/acp-19-8703-2019, 2019.

Xing, J., Wang, J., Mathur, R., Wang, S., Sarwar, G., Pleim, J., Hogrefe, C., Zhang, Y., Jiang, J., Wong, D., and Hao, J.: Impacts of aerosol direct effects on tropospheric ozone through changes in atmospheric dynamics and photolysis rates. Atmos. Chem. Phys., 17, 9869 – 9883, https://doi.org/10.5194/acp-17-9869-2017, 2017.Zhang, H., Zhang, X., Li, Q., Cai, X., Fan, S., Song, Y., Hu, F., Che, H., Quan, J., Kang, L., and Zhu, T.: Research progress on estimation of the atmospheric boundary layer height, J. Meteor. Res., 34, 482–498, https://doi.org/10.1007/s13351-020-9910-3, 2020.

Zhang,.L, Gong, S., Padro, J., and Barrie, L.: A size-segregated particle dry deposition scheme for an atmospheric aerosol module, Atmos. Environ., 35, 549–560, https://doi.org/10.1016/S1352-2310(00)00326-5, 2001.

Zhang, X., Xu, X., Ding, Y., Liu, Y., Zhang, H., Wang, Y., and Zhong, J.: The impact of meteorological changes from 2013 to 2017 on PM$_{2.5}$ mass reduction in key regions in China, Sci. China Earth Sci., 62, 1–18. https://doi.org/10.1007/s11430-019-9343-3, 2019.
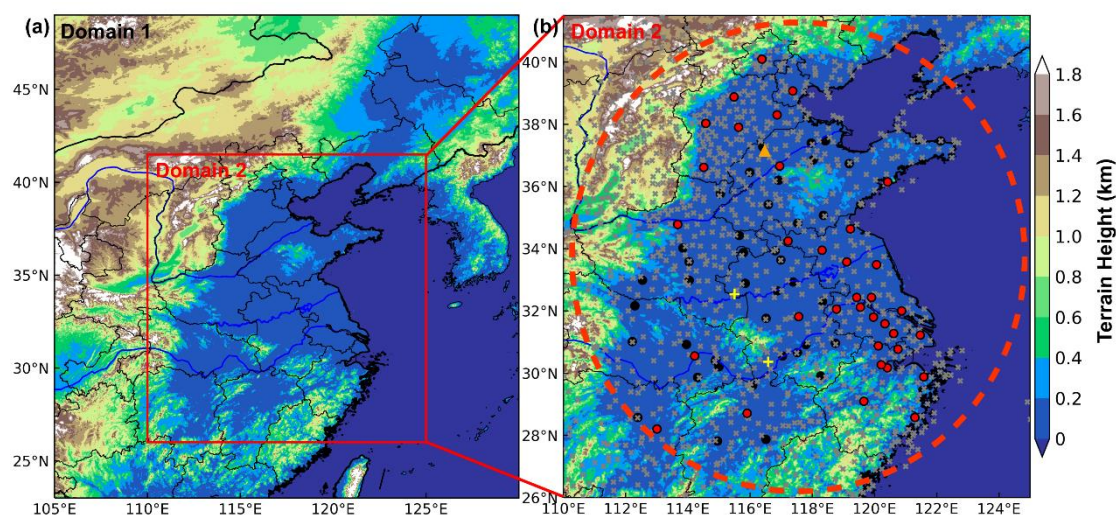
Figure 1. (a) Map of terrain height in the two nested model domains. (b) The locations of surface meteorological stations, air quality monitoring stations and sounding stations are marked by the gray crosses, red(black) dots and yellow pluses, respectively. The turbulence data site is denoted by the orange triangle. The red dashed circle indicates the areas of our primary concern.
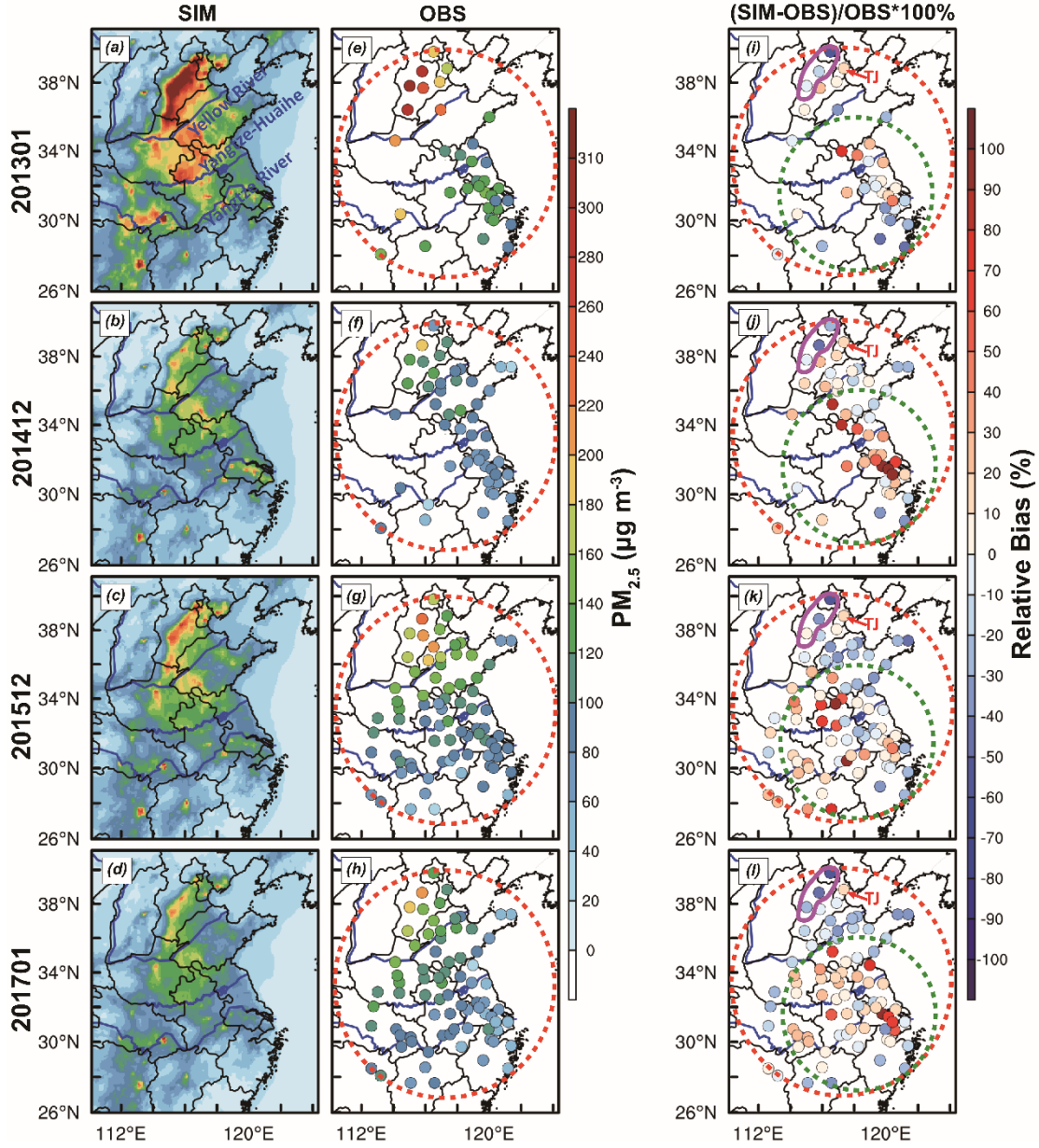
Figure 2. The average value of (a-d) simulated and (e-h) observed PM₂.₅ concentration (μg m⁻³) at night, (i-l) the relative bias (RB, %) between simulation and observation, and the calculation formula of relative bias is $RB = \left(\overline{X_{sim}} - \overline{X_{obs}} \right) \big/ \overline{X_{obs}} \times 100\%$ **, where** $\overline{X_{sim}}$ **and** $\overline{X_{obs}}$ **represent the average value of simulation and observation, respectively. The locations of three rivers (i.e., Yellow River, Yangtze-Huaihe and Yangtze River) are marked by blue lines. The red and green dashed circles represent the whole simulation area and Eastern China, respectively. The purple solid irregular circle indicates mountainous areas, and the red text TJ indicates Tianjin.**
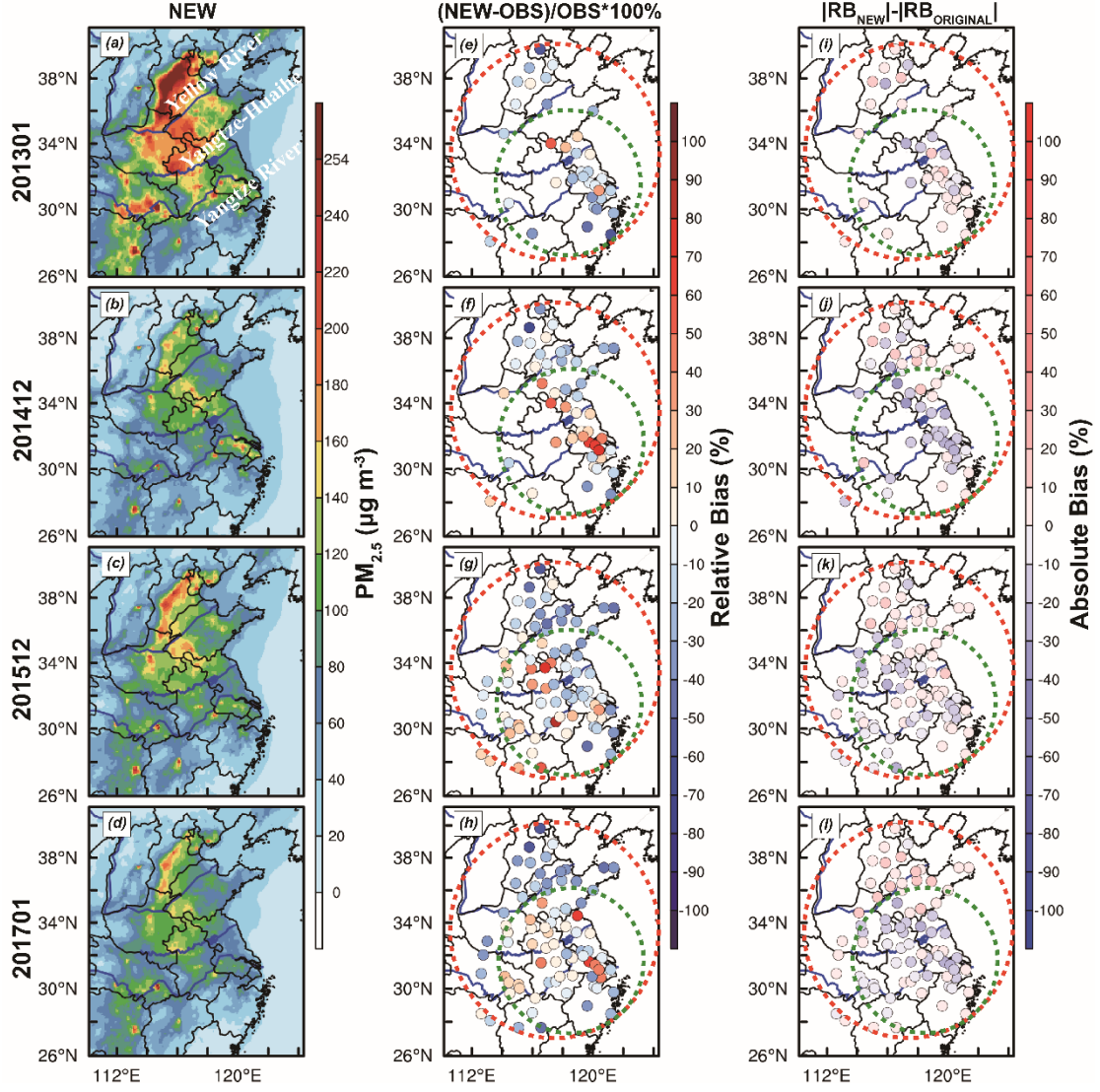
Figure 3. The average value of (a-d) simulated PM$_{2.5}$ concentration (μg m^{-3}) by new schemes, (e-h) the relative bias (RB, %) of PM$_{2.5}$ concentration between simulation of new scheme and observation, (i-l) the absolute bias (AB, %) between new and original schemes, and the calculation formula of absolute bias is $AB = \left| RB_{new} \right| - \left| RB_{original} \right|$, where $\left| RB_{new} \right|$ and $\left| RB_{original} \right|$ represent the relative bias of new and original schemes, respectively. The red and green dashed circles represent the whole simulation area and Eastern China, respectively.
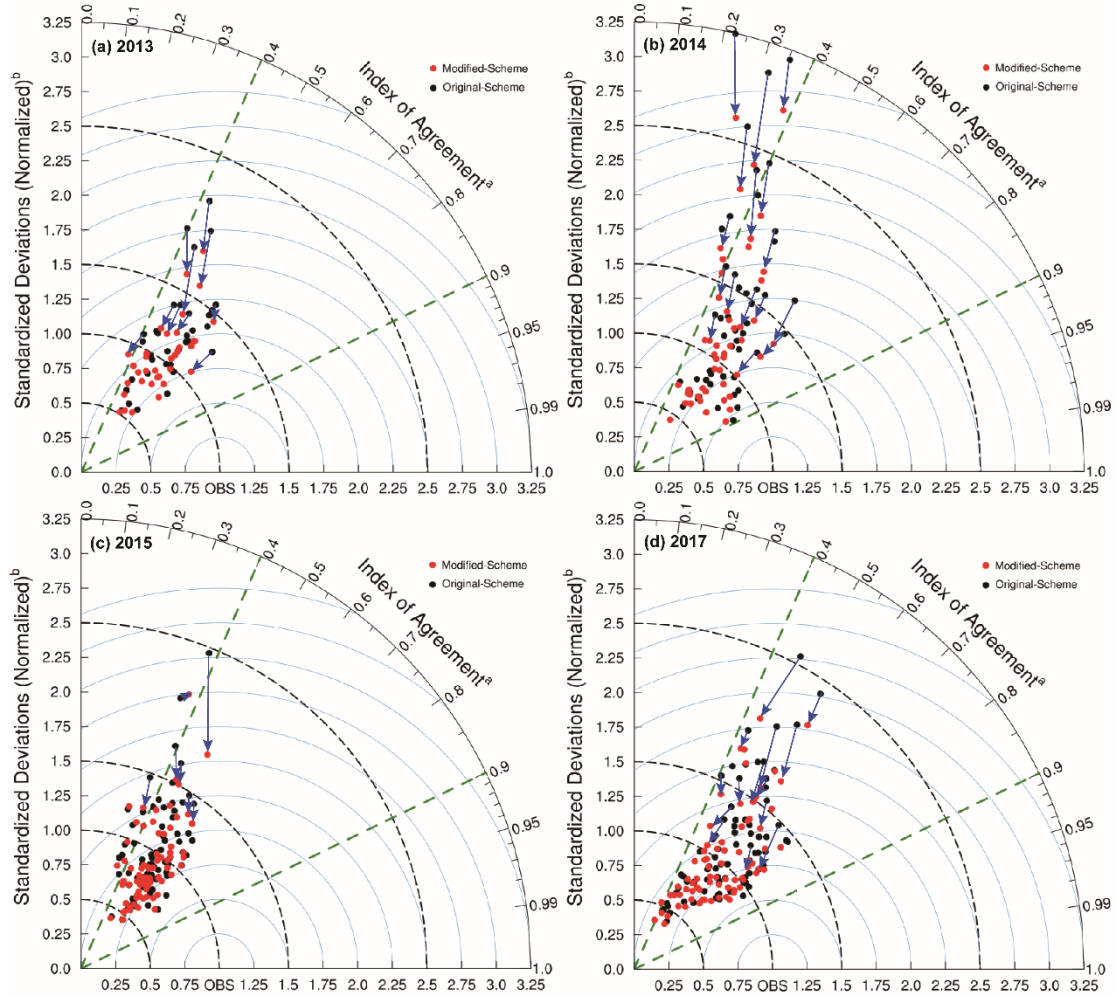
Figure 4. Taylor diagram of simulation by original scheme and modified scheme. XY axes and arc represent the normalized standardized deviations (NSTD,

$$\text{NSTD} = \frac{\sqrt{\dfrac{1}{N-1}\sum_{i=1}^{n}\left(X_{\text{sim},i} - \overline{X_{\text{sim}}}\right)^2}}{\sqrt{\dfrac{1}{N-1}\sum_{i=1}^{n}\left(X_{\text{obs},i} - \overline{X_{\text{obs}}}\right)^2}} , \; \overline{X_{\text{sim}}} \; \text{and} \; \overline{X_{\text{obs}}} \; \text{represent the average value of}$$

640 **simulation and observation, respectively) and index of agreement (IOA,**

$$\text{IOA} = 1 - \frac{\left[\sum_{i=1}^{n}|X_{\text{sim},i} - X_{\text{obs},i}|^2\right]}{\left[\sum_{i=1}^{n}(|X_{\text{sim},i} - \overline{X_{\text{obs}}}| + |X_{\text{obs},i} - \overline{X_{\text{obs}}}|)^2\right]} , \; X_{\text{sim,i}} \text{ and } X_{\text{obs,i}} \text{ represent the value of}$$

simulated and observed, respectively. i refers to time and n is the total number of time series), respectively. All cities (a total of 35 cities in 2013 and 78 cities in 2014, 2015 and 2017) are shown through dots, and black (red) represents original (new) scheme. The root mean square (RMS) is

645 **denoted by blue dashed line and the arrow indicates the change of the new scheme compared to the original scheme at the same station.**
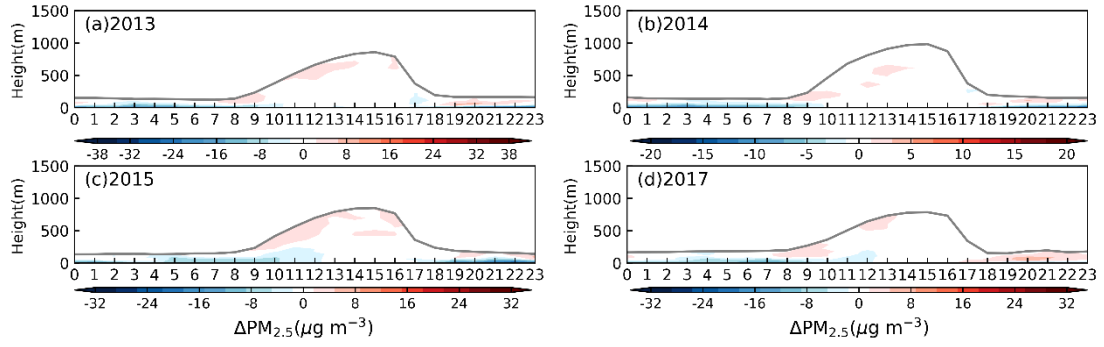
Figure 5. Time-height cross sections for the difference of PM$_{2.5}$ concentration between original and new schemes (i.e., the new scheme minus the original scheme) within the PBL. The gray line indicates the PBLH.
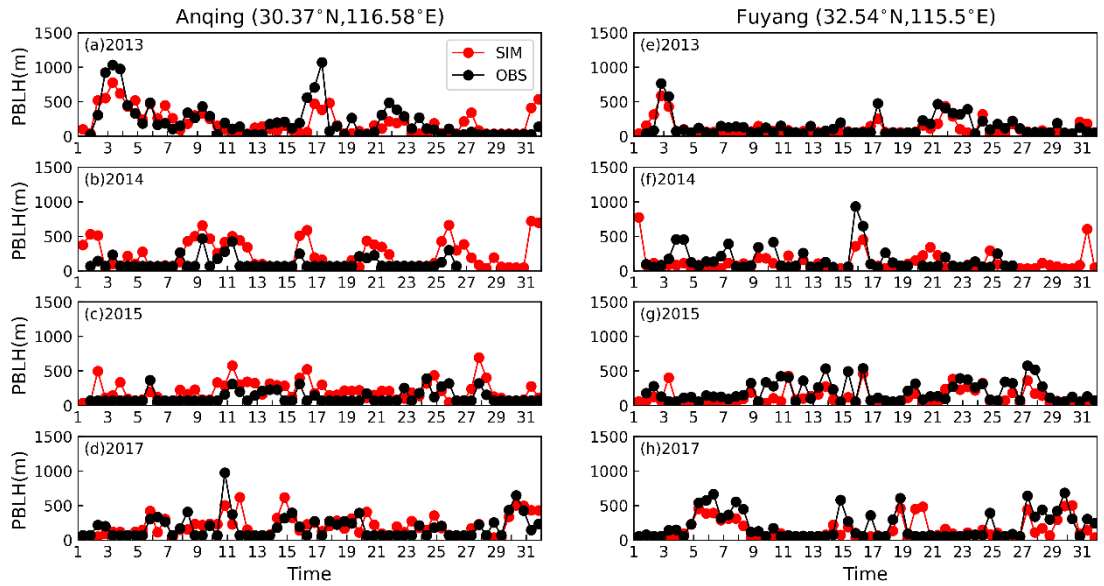
Figure 6. Time series of the observed (black) and simulated (red) PBLH at 0800 and 2000 (BJT) in the (a-d) Anqing and (e-h) Fuyang from 2013 to 2017.
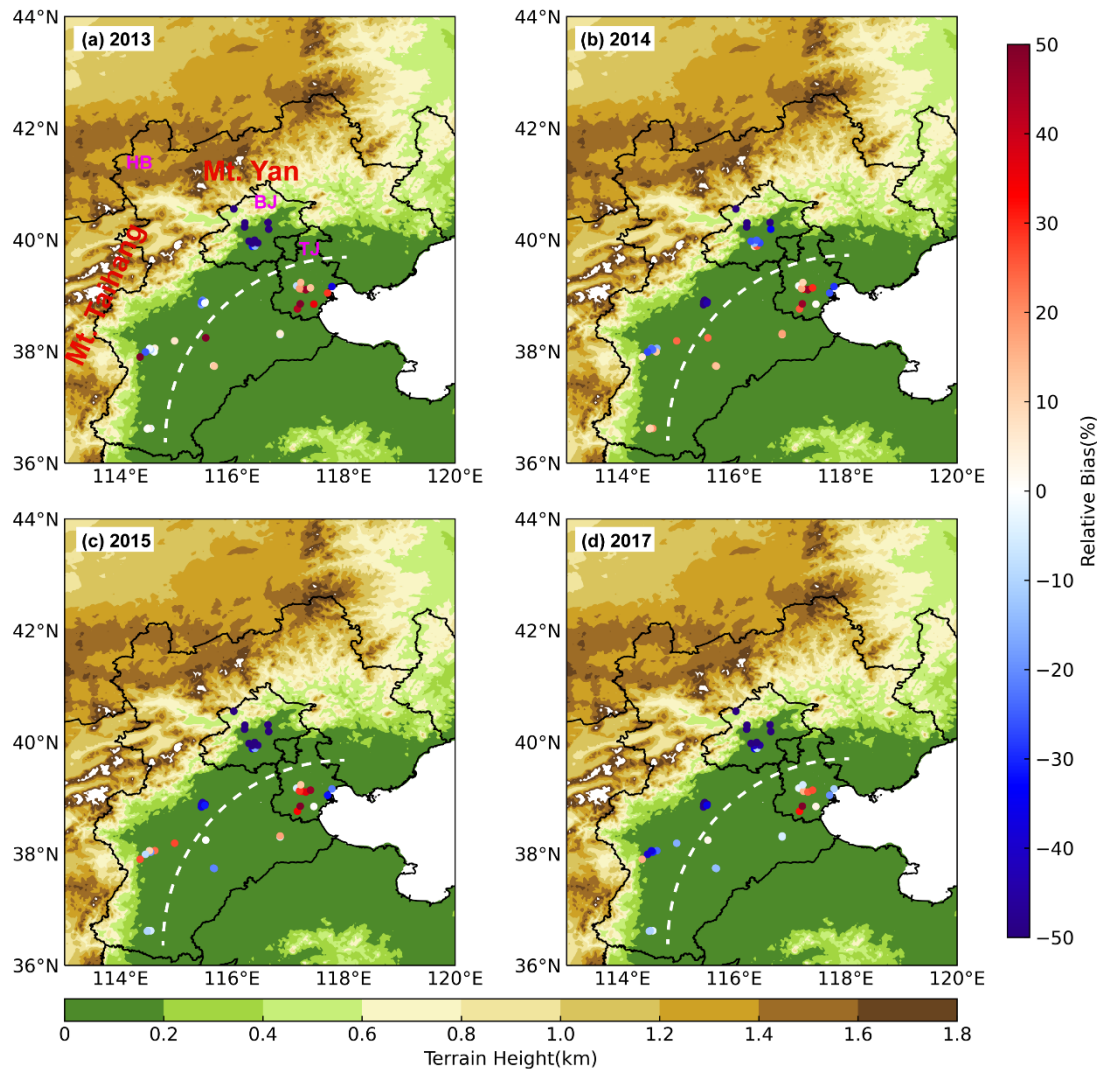
Figure 7. The relative bias (%) between simulation and observation at all environment monitoring stations and terrain height in Beijing-Tianjin-Hebei in (a) 2013, (b) 2014, (c) 2015 and (d) 2017. Taihang Mountain (Mt. Taihang) and Yanshan Mountain (Mt. Yan) are indicated by red text, Beijing (BJ), Tianjin (TJ) and Hebei (HB) are represented by purple abbreviation and the dividing line between overestimated and underestimated areas is indicated by a white dashed line.
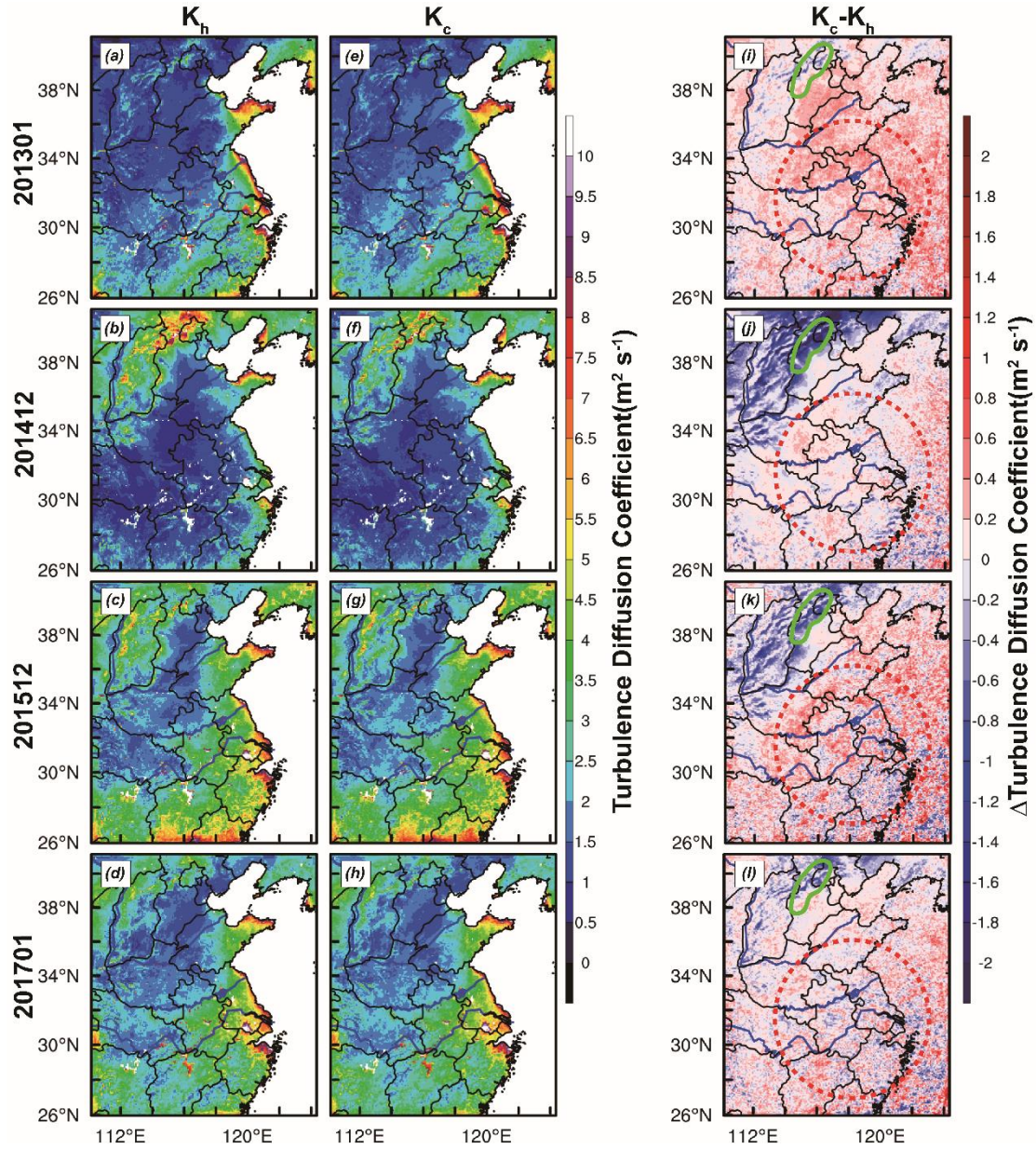
Figure 8. Turbulent diffusion coefficient of (a-d) heat and (e-h) particles, and (i-l) the difference between two turbulent diffusion coefficients. The red dashed and green solid irregular circles represent Eastern China and mountainous areas, respectively.
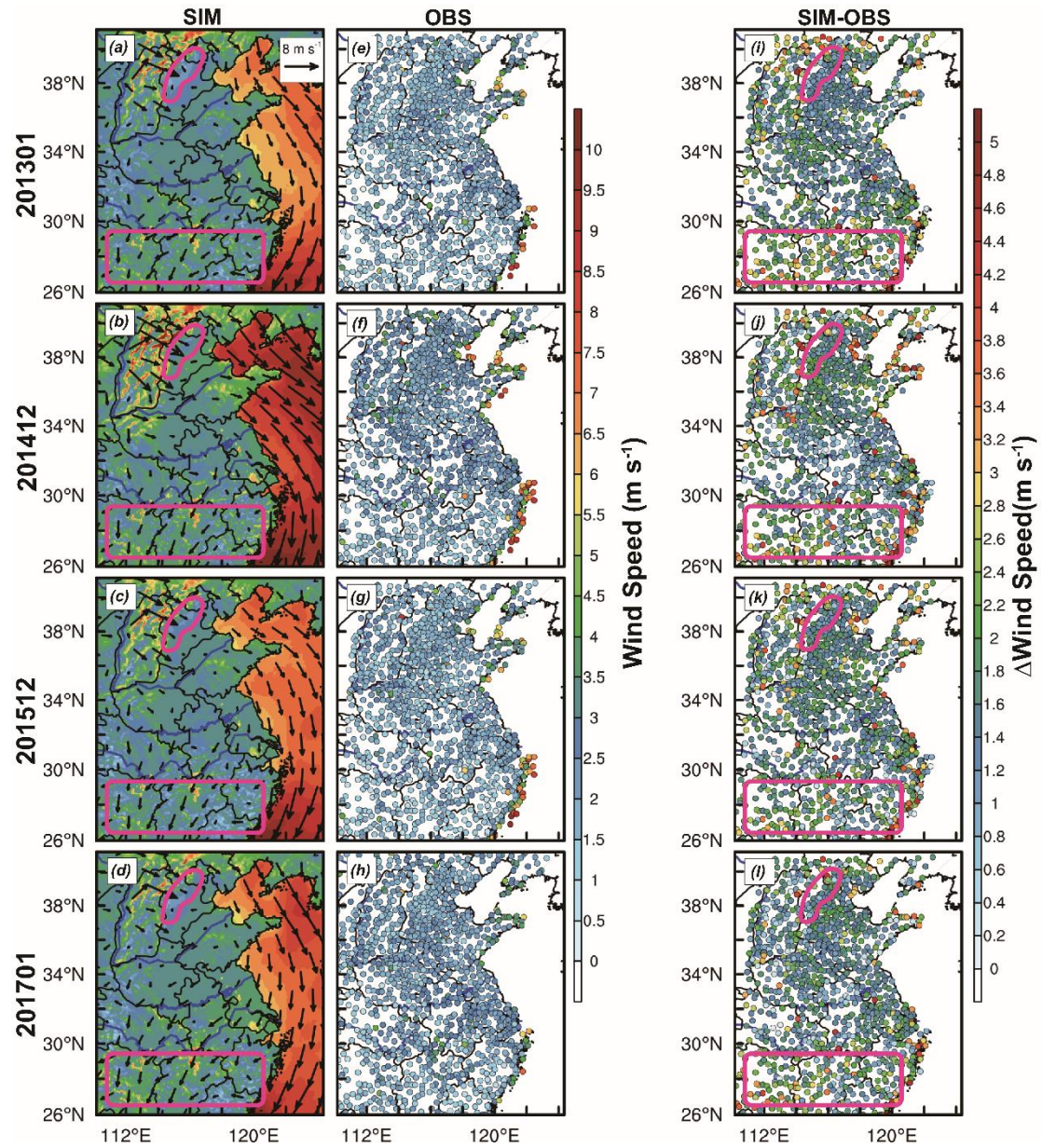
Figure 9. (a-d) Simulated and (e-h) observed wind speed at 10 m above ground level (AGL), and (i-l) the difference of simulated and observed. The purple rectangle indicates the area where the observed wind speed is significantly overestimated.